

Effect of Mold Cooling Intensity on the Depression-Type Crack Formation and Mold Flux Infiltration During Continuous Casting Process



FENGGANG WANG, HANG HE, WANLIN WANG, LEI ZHANG, JIAXI CHEN, JIANG DU, and JIE ZENG

As one of the most serious defects in the products of continuous casting steel, the surface depressions with longitudinal cracks originated from the mold were clearly characterized. A mold simulator technique was developed to investigate the effects of different mold cooling flow rates (3.5, 6.0, 7.5 L/min) on the evolution of depression-type cracks and mold flux infiltration for the steel continuous casting in this study. The mold simulator results indicated that the depression and longitudinal crack become more serious with the increasing of mold cooling intensities. Furthermore, when the cooling intensity enhanced from 3.5 to 7.5 L/min, the average solidification factor of shell increased rapidly from 2.37 to 2.91 (mm/s)^{1/2}, and the mean heat flux in the initial solidified shells with depressions reduced by 0.723 MW/m² during the initial 0 to 1.5 seconds solidification stage. In addition, the higher mold cooling intensities of 6.0 to 7.5 L/min could result in an increasing of slag film thickness and the formation of amorphous slag, which contributed to the uneven infiltration of mold flux.

<https://doi.org/10.1007/s11663-023-02911-4>

© The Minerals, Metals & Materials Society and ASM International 2023

I. INTRODUCTION

THE steel materials have been widely used in various fields such as national defense industry, machinery, construction, automobile, shipbuilding, home appliances, etc. due to its superior comprehensive mechanical properties^[1-4] But surface cracks in continuous casting steel have become a serious quality defect, which significantly affects production efficiency and product quality.^[5-8] Complex, high-temperature, multiphase, transient physicochemical changes occur in the continuous casting mold, which constrains the study of the formation mechanism of depressions and cracks on the surface of the continuous casting steel.

It has been widely accepted that surface defects of continuous casting steel relates to pouring temperature, casting speed, mold conditions, mold water cooling, taper of mold, mold oscillation, mold flux *etc.*^[9-16] In which, the mold water cooling intensity is one of the most important factors, which significantly affects surface quality of products.^[17,18] Murakami *et al.*^[18] pointed out that the larger water cooling leads to the formation of solidified shell depressions at the initial solidification stage of steel. Mahapatra^[15] suggested that cooling water intensities may have an impact on surface cracks as well. Besides, the surface cracking and depression problems often correspond to the mismatches between solidification contraction and mold taper.^[13,19-23] Tomas *et al.*^[14,22,23] calculated that an increasing interfacial gap between the solid shell and mold can cause locally hot and thin portions of the shell due to a reduction of heat transfer between the shell and mold.

On the other hand, cooling rates have significantly impacts on the infiltration of liquid slag and the crystallization of the slag film, and they play an important role to lubrication and heat transfer during continuous casting process, and then affect the surface quality of cast products.^[24,25] Thomas *et al.*^[26] suggested that an uneven infiltration of molten slag could worsen the irregular shell solidification and mold flux entrapment, and thus, many surface defects, such as ripples and deep oscillation marks, were formed on the

FENGGANG WANG, HANG HE, WANLIN WANG, LEI ZHANG, JIAXI CHEN, and JIE ZENG is with the School of Metallurgy and Environment, Central South University, Changsha 410083, P.R. China and also with the National Center for International Research of Clean Metallurgy, Central South University, Changsha 410083, P.R. China. Contact e-mail: jie.zeng@csu.edu.cn JIANG DU is with the Xiangtan Iron & Steel Co., Ltd. of Hunan, Xiangtan 411101, P.R. China.

Manuscript submitted May 16, 2023; accepted August 24, 2023.

Article published online September 15, 2023.

non-uniform solidified shell. In addition, Yang *et al.*^[27] found that the composition inhomogeneity of the mold flux film can cause large fluctuations of the heat flux in the mold, resulting in the appearance of irregular depressions on the shell surface.

However, some works have been investigated formation of depressions by dip test due to uneven solidified shell formation at the initial stage of solidification, which lacks especially of detailed correlation of depression-transient heat flow-slag film behavior, *etc.*^[15,18] Besides, evolution of depression-type cracks was investigated by numerical simulation which lacked of experimental verification.^[14,22,23] In this study, to reveal the relationships between the depression-type cracks, mold cooling intensities, heat transfer, infiltration, and crystallization behavior of the mold flux during steel continuous casting, a mold simulator technique was developed to investigate the effects of different mold cooling intensities (3.5, 6.0, 7.5 L/min) on the evolution of depression-type cracks and mold flux infiltration in steel continuous casting.

II. EXPERIMENTAL MATERIALS AND APPARATUS

A. Analysis of Surface Defects of Bloom

In the current study, medium carbon-alloyed steel was used. Table I shows the chemical composition of this steel. The medium carbon-alloyed steel was obtained from the first strand of a bloom continuous caster with a section size of 350 mm × 430 mm, and the casting machine in this plant is the straight-arc bloom continuous casting machine of four strands. The surface cracks specimens with a size of 15 × 15 × 15 mm were taken from the wide surface of the bloom. Besides, surface cracks specimens with depressions were analyzed by the three-dimensional (3D) depth of field (KEYENCE, Japan, VHX-5000) to understand the macroscopic characteristics of cracks. Moreover, the surface cracks specimens sectioned from bloom were ground, polished, and etched with a 4 pct nital nitric acid solution or saturated picric acid solutions, and observed by an optical microscope (OM, Leica DM4 M, Germany) and a scanning electron microscopy (SEM, TESCANMIRA 3 LMU, Czech Republic) equipped with an X-ray energy-dispersive spectrometer (EDS).

Table I. The Chemical Compositions of the Medium-Carbon Sulfur Containing Steel (Weight Percent)

C	Mn	Si	Cr	S	Mo	P	Al
0.38 to 0.40	0.66 to 0.76	0.20 to 0.30	1.12 to 1.18	0.0249	0.018 to 0.022	0.016 to 0.020	0.01 to 0.02

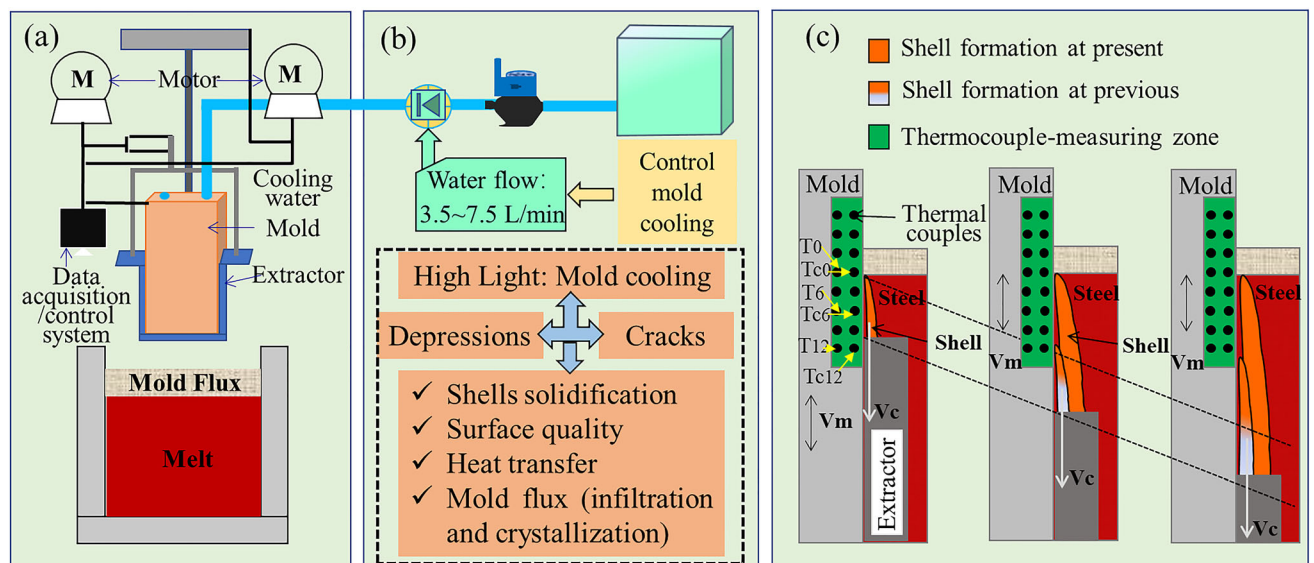


Fig. 1—The schematic diagram of the mold simulator apparatus: (a) schematic diagram of equipment, (b) Mold cooling system, (c) Initial solidification process of molten steel.

Table II. The Chemical Compositions of the Mold Fluxes (Weight Percent)

SiO ₂	CaO	Al ₂ O ₃	MgO	MnO	Na ₂ O	F ⁻	C _{total}
24 to 26	28 to 30	8 to 10	2 to 3	2 to 3	4 to 6	4 to 6	14 to 16

B. Mold Simulator Experiment

As an experimental material, the medium carbon-alloyed steel was applied for the mold simulator experiment. The mold simulator used in this study is an inverse-type water-cooled copper mold, as shown in Figure 1(a). The detailed experimental configuration and its operational steps have been reported in our previous study.^[28–31] The mold simulator process mainly includes (1) Melting of the medium carbon-alloyed steel; (2) Adding mold flux after steel melting, the chemical compositions of mold flux used during the mold simulator experiment are presented in Table II; (3) Simulating continuous casting process with an identical casting speed V_c of 10 mm/s, a stroke of 4.7 mm, and a frequency of 165 cpm. Besides, V_m means copper mold velocity, and the degree of superheat is controlled with a value of 30 °C in the laboratory mold simulator; (4) Cutting away the solidified shell from the copper mold for analyzing the surface quality and obtaining the mold flux films between copper mold and solidified shell. The dates of heat flux were obtained by a 2D-IHCP of converting the measured date history of thermocouples.^[29] Moreover, in order to investigate the effects of mold cooling intensities on the initial solidification behavior of the sulfur-containing steel continuous casting, different mold cooling water flows (3.5, 6.0, 7.5 L/min) were applied.

Similarly, the surface defects of obtained shell from mold simulator experiment were analyzed by the three-dimensional (3D) depth of field. The surface cracks specimens sectioned from the mold simulator experiment and bloom were ground, polished, and etched with a 4 pct nitric acid solution or saturated picric acid solution, and observed by OM and SEM-EDS. Moreover, the X-ray diffraction (XRD, Rigaku SmartLab, Japan, TTR III) and SEM-EDS were employed to identify the phase compositions and morphology of crystals precipitated from the mold flux films.

C. Continuous Cooling Transformation Diagram of Mold Flux

In addition, the continuous cooling transformation (CCT) diagram was measured using the single hot thermocouple technology (SHTT) to determine the initial crystallization temperature of mold flux under different cooling rates. The mold flux using pure chemicals was melted in a graphite crucible, which was placed into an induction furnace, at 1773 K (1500 °C) for 300 seconds to homogenize its chemical composition and eliminate bubbles. Then, the mold flux was poured into water for quenching to obtain fully glassy phase

flux. Next, the glassy sample was dried, crushed, and ground into sample powders for the following single hot thermocouple technology (SHTT) test.

III. RESULTS AND DISCUSSION

A. Analysis on the Surface Defects of the Industrial Bloom

The macroscopic morphology of the cracks and depressions on the wide surface of bloom with a section size of 430 × 350 mm is shown in Figure 2. It can be seen from Figure 2(a) that the depressions are along the casting direction, and cracks are formed at the valley of the depressions. It also can be observed from Figure 2(b) by the 3D depth of field that the maximum length of depressions was about 13 cm and depressions depth reached about 0.5 cm. Moreover, it was obvious that the surface cracks were formed along the longitudinal depressions, as shown in Figures 2(a) and (b). Further, OM analysis (Figure 2(c)) from surface of crack indicated that the solidified dendrites near the crack became larger, which indicated the heat transfer near the cracks was slower compared to the matrix. OM analysis (Figures 2(c1) and (c2)) from longitudinal cross section of crack indicated that there are obvious decarburization layer and the depth of decarburization layer could reach about 400 μm. Therefore, it can be inferred that the longitudinal cracks on the surface were generated in the mold due to formation of depressions, changes of heat transfer, and generation of obvious decarburization layer.^[14,15] Thus, it is indicated that formation of the depression-type cracks are closely related to initial solidified behavior of liquid steel in the vicinity of the mold meniscus, including mold cooling intensities, heat transfer, infiltration, and crystallization behavior of the mold flux during steel continuous casting.

B. Effect of Mold Cooling Intensity on Surface Quality of Solidified Shells and the Infiltration of Mold Flux

Figure 3 shows the surface of the solidified shells and the distribution of the slag films with different cooling intensities by mold simulator experiment. It can be seen that the shell surface is clean and flat, the distribution of slag film is also relatively uniform when the cooling intensity is relatively low with the cooling water flow rate of 3.5 L/min. When the cooling water flow rate increases to 6.0 L/min, transverse depressions in the surface shell are generated, and the distribution of the slag film becomes uneven. As shown in Figure 3(c), the surface shell with severe (transverse and longitudinal) depressions and more uneven slag film can be observed

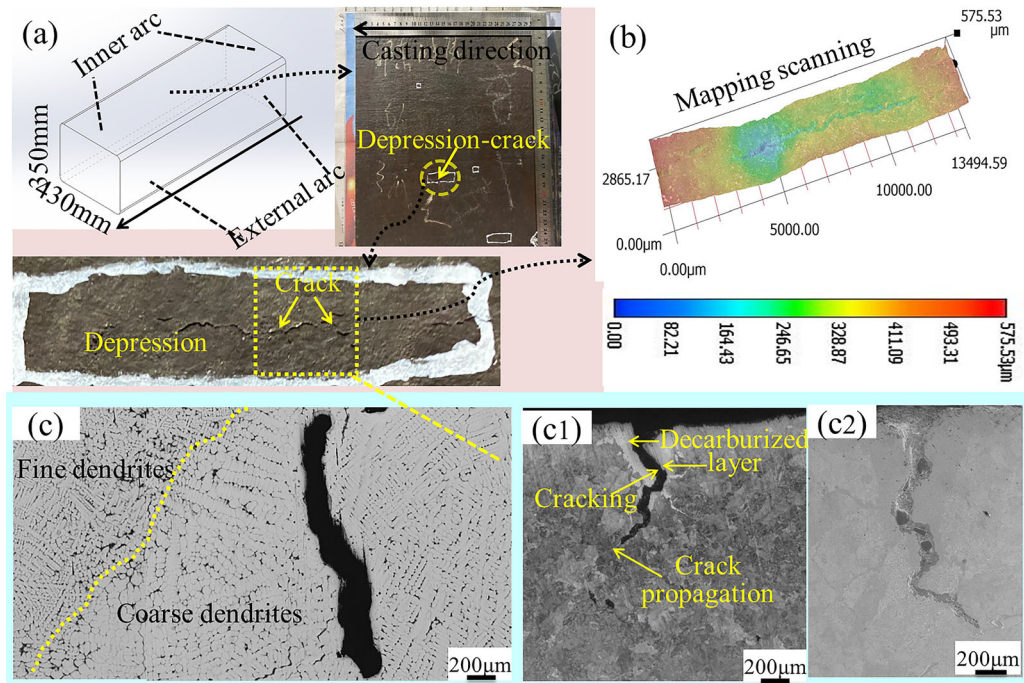


Fig. 2—Characteristics of surface cracks in the bloom: (a) Macroscopic of surface depression-type crack, (b) 3D depth of field of depressions, (c) Dendrite of crack surface, (c1) OM from longitudinal cross section of crack, (c2) SEM from longitudinal cross section of crack.

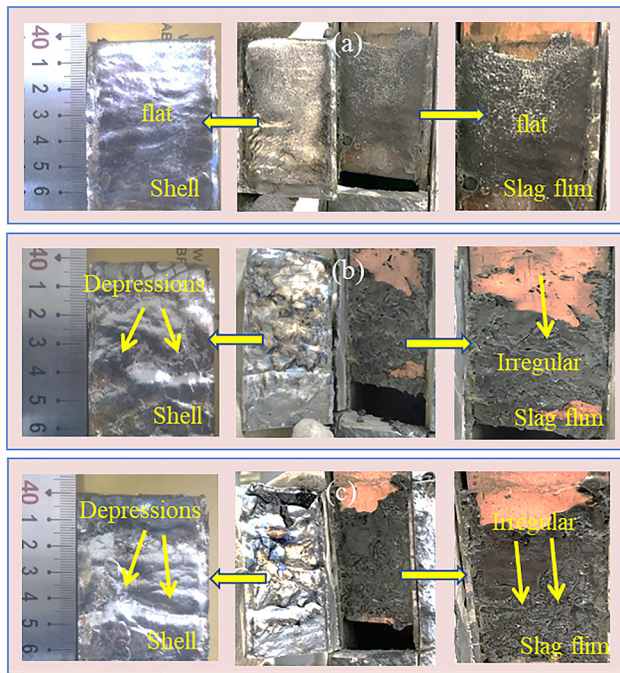


Fig. 3—The surface quality of shells and slag films under different cooling intensities: (a) 3.5 L/min, (b) 6.0 L/min, (c) 7.5 L/min.

when the cooling water flow rate was further enhanced to 7.5 L/min. In addition, the 3D depth-of-field analysis of the depressions obtained from the surface of the initial solidification shells is further shown in Figure 4.

When the cooling water flow rate was 7.5, 6.5, and 3.5 L/min, the depth of depressions on the surface of the shell was 1200, 900, and 100 μm , respectively. It was reported that the deeper depressions may lead to an uneven penetration of the mold flux due to the changing of physical and chemical properties of the mold flux caused by excessive mold cooling intensity.^[12,13,21,23,32] Thus, the appropriate mold cooling intensities are a significant factor that can ensure even infiltration of mold flux and high surface quality of the solidified shell. Therefore, it was obvious that increasing of the mold cooling intensities from 3.5 to 7.5 L/min can result in the formation of depressions and the uneven infiltration of liquid mold flux.

Moreover, when the cooling water flow rate was 3.5 L/min, no cracks are found on the flat shell surface. In comparison, as shown in Figure 5(a), the longitudinal crack with a depth of 1722 μm formed at the position of the depression when the cooling water flow rate was 6.0 L/min. When the cooling water flow increased to 7.5 L/min, the serious cracks with a depth of 3267 μm appeared in Figure 5(b). Therefore, it can be concluded that when the mold cooling intensity becomes too high, it can cause the formation of longitudinal cracks accompanied by the depressions. Meanwhile, as the increasing of the depressions, the heat transfer between the mold plate and steel shell reduced, which leads to the formation of locally hot and thin portions of the shell,^[7,23,33,34] and then may lead to the formation of surface crack due to stress concentration. Besides, uneven solidified shell (depression and crack) may lead to the phenomenon of sulfur enrichment and formation

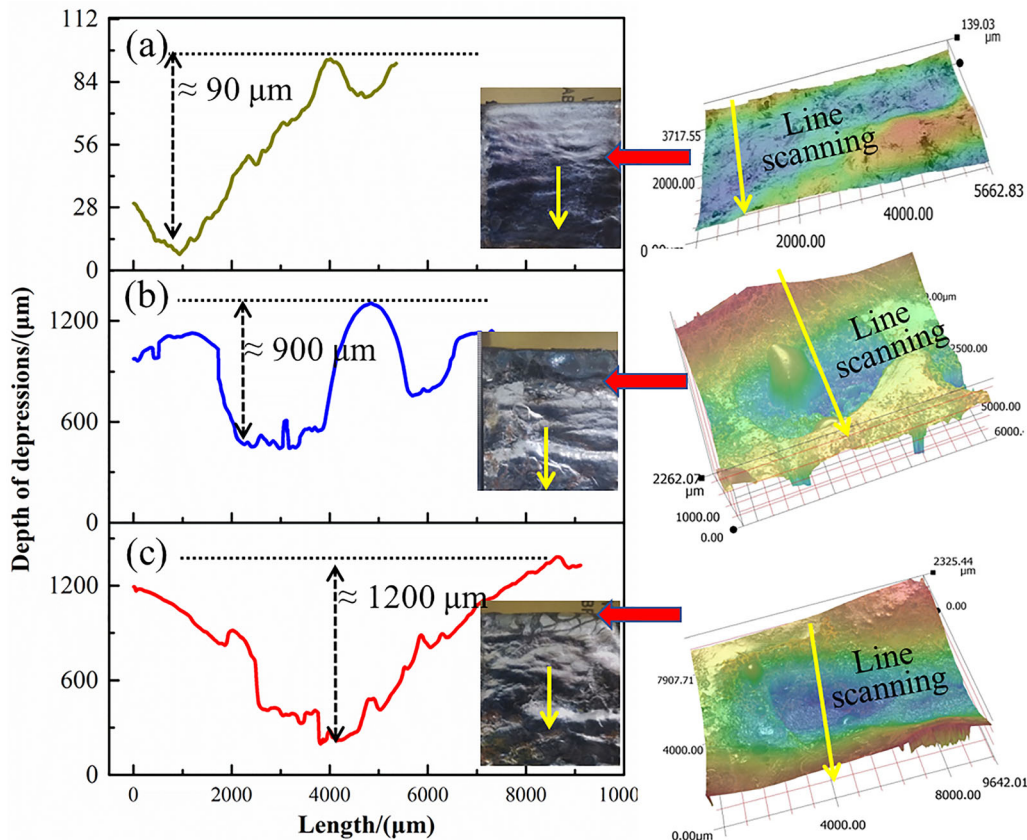


Fig.4—The lengths of depressions on shell surface under different cooling intensities: (a) 3.5 L/min, (b) 6.0 L/min, (c) 7.5 L/min.

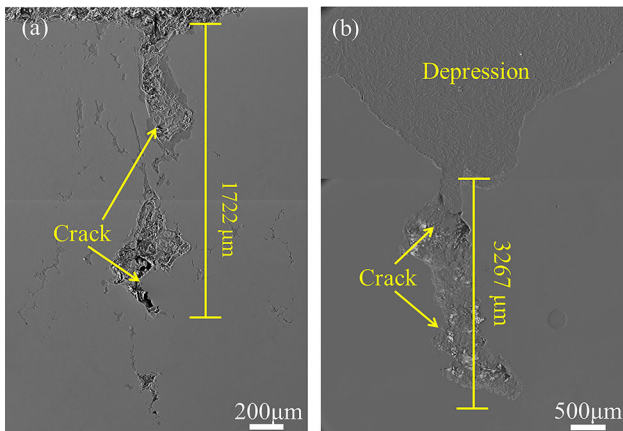


Fig. 5—The microscopic characteristics of solidified shells with surface cracks: (a) 6.0 L/min, (b) 7.5 L/min.

MnS inclusions in the area of crack. Xing *et al.* found clearly MnS inclusions formed in the area of crack in medium carbon sulfur-containing alloyed bloom.^[5–7,33] Regrettably, the chemical compositions of the shell in the area of crack remain essentially unchanged in this study. Especially, the phenomenon of sulfur enrichment

is not very obvious due to the larger cooling rate in the surface. It is worth paying attention to the chemical compositions of shell in the area of crack and depression should be significantly presented in some work, especially that steel grade consists of elevated level of sulfur.

C. Effect of Mold Cooling Intensity on Heat Transfer and Shell Thickness

The solidification rates of the initial shell mainly depended on the steel grade and the mold simulator casting conditions. As shown in Figure 6(a), the longitudinal section of the solidified shells can be obtained after the mold simulator experiments under different mold cooling intensities. The thickness (s) of shell versus time (t) is fitted with a solidification square root law $s = K\sqrt{t}$ (K is time-average solidification factor), as shown in Figure 7(b). Besides, the instantaneous solidification rate (K_t) can be calculated by equation K_t/s . According to the fitting results, it is calculated that the average solidification factor of shell under mold cooling water flow rates of 3.5, 6.5, and 7.5 L/min is 2.37, 2.83, and 2.91 (mm/s)^{1/2}, respectively. It indicated that the growing of shell was faster during the initial solidification of the sulfur-containing steel with the enhanced mold cooling intensity.

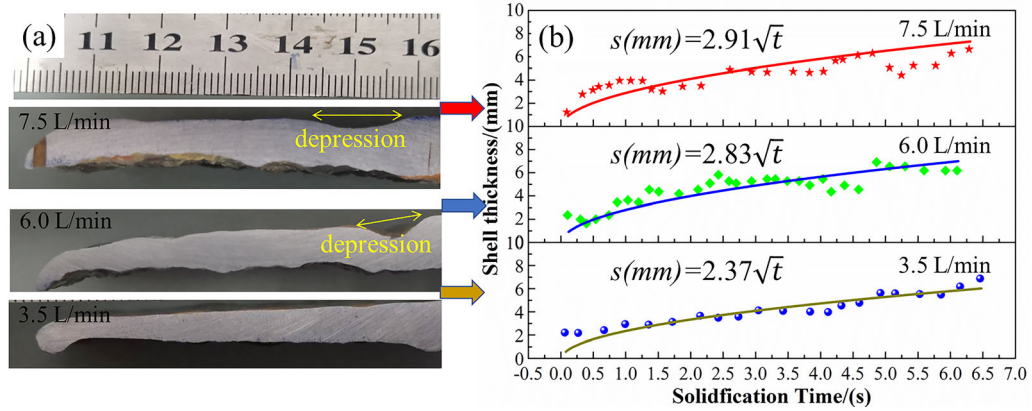


Fig. 6—Solidified shell and thickness fitting of shell under different mold cooling intensities: (a) Solidified shell of longitudinal cross section, (b) Thickness fitting of shell.

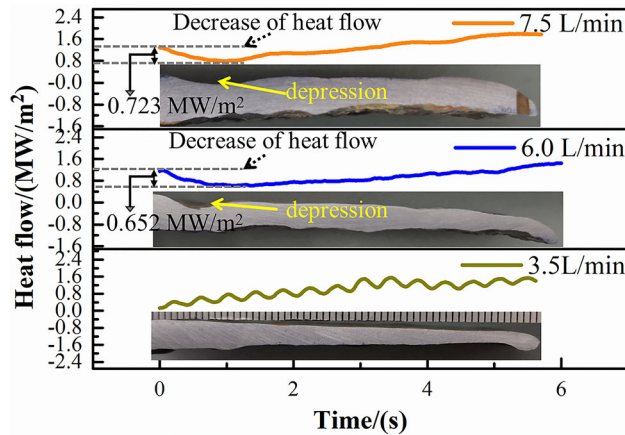


Fig. 7—Heat flow density at the mold meniscus under different cooling intensities.

In order to further analyze the effect of mold cooling intensities on the heat transfer of the initial solidification of steel, the heat flow at the mold meniscus under various water flow rates of 3.5 to 7.5 L/min were analyzed. As shown in Figure 7, when the cooling water flow decreased to 3.5 L/min, no obvious depressions appear in the initial solidification shell due to a slowly heat flow. In comparison, when the cooling water flow increased to 6.0 L/min, the heat flow of shell with depression reduced by 0.652 MW/m² during the initial 1.0 second stage of solidification. Moreover, the heat transfer in the solidification shell surface with depression reduced by 0.723 MW/m² during the initial 1.5 seconds solidification stage of the steel in a cooling condition of 7.5 L/min. Thus, the formation of depressions can cause a significant reduction of heat flow between mold and solidification shell when the mold cooling intensity becomes too high.

D. Effect of Mold Cooling on the Infiltration and Crystallization of Mold Flux

The mold cooling intensity acts as an important role in the structure and distribution of slag layer. As shown in Figure 8, the thickness of the slag film was about 1.92 mm under the cooling water flow of 7.5 L/min. As shown in Figures 8(d) through (f), when the cooling water flow was reduced to 3.5 L/min, the thickness of the slag film gradually decreased with the decreasing of mold cooling intensities.

Furthermore, the XRD analysis of the slag films under different cooling intensities was conducted. When cooling water flow was 3.5 L/min, the slag film mainly contained the phase of Ca₂SiO₄, CaMg(SiO₄)₂, and Ca_{1.7}Mg_{0.3}SiO₄, combining the results of the mapping scanning in Figure 9. In comparison, it was obvious that the non-crystalline slag films formed under cooling rates of 7.5 and 6.0 L/min. Thus, in order to determine the formation of amorphous slag layer, the non-isothermal CCT curves were conducted by single hot thermocouple tests. As shown in Figure 10, the initial crystallization temperature of mold fluxes decreased gradually from 1319 °C to 1208 °C when the cooling rates increased from 1.0 °C/s to 3.0 °C/s. As expected, it has been reported that the time and temperature for the beginning of crystallization decreased with increasing cooling rates, and for cooling rates greater than a value, no crystallization was observed indicating that the critical cooling rate for mold slags was reached.^[35] It was found that the critical cooling rates of glass phase transition for this mold flux were about 3.0 °C/s to 3.5 °C/s. Therefore, on the basis of satisfying the physicochemical properties (chemical composition, viscosity, density, break point, crystallization and heat transfer *etc.*) of the mold flux in the production of bloom, critical cooling rates may be a valid way for considered flux, which should be avoided to formation of non-crystalline slag films.

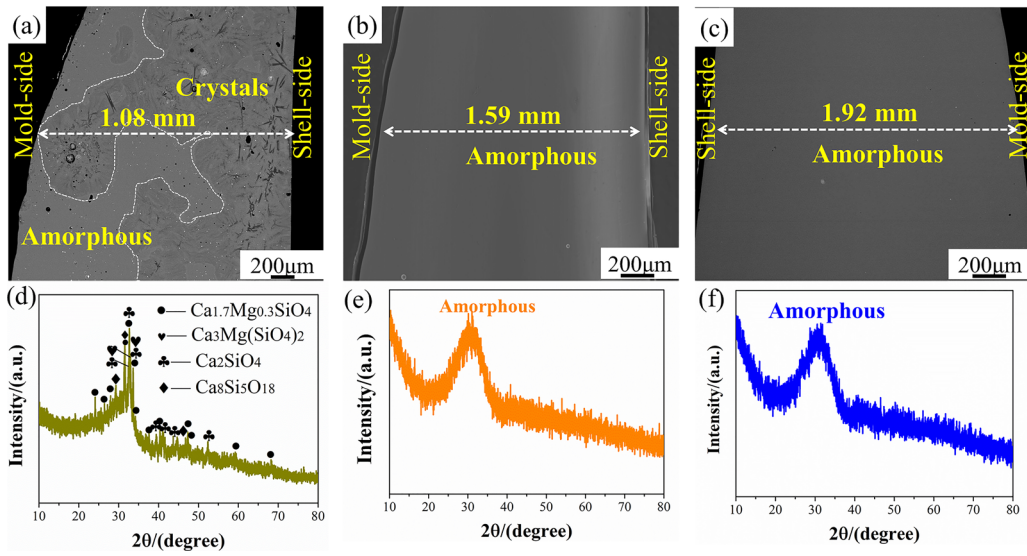


Fig. 8—The structure and distribution of mold flux at the mold meniscus under different cooling intensities: (a, d) 3.5 L/min, (b, e) 6.0 L/min, (c, f) 7.5 L/min.

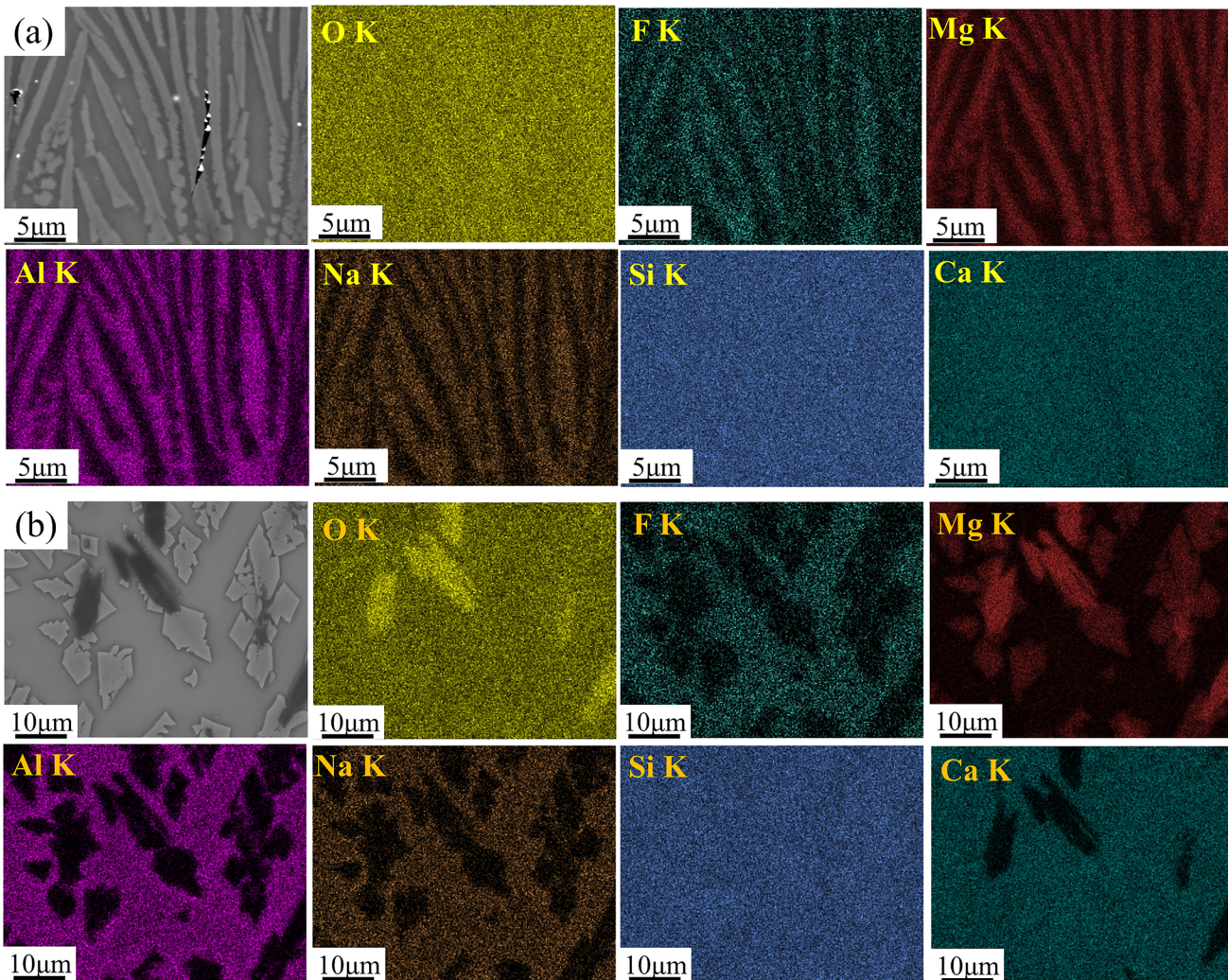


Fig. 9—The typical microstructure of mold flux under a cooling water flow of 3.5 L/min: (a) phases of Mg-Si-Ca-O rich, (b) phases of Mg-Si-O rich and Ca-Si-O rich.

E. Formation Mechanisms of Depression-Type Cracks in Continuous Casting Steel

The formation mechanisms of depression-type cracks in continuous casting steel were clarified by analyzing the relationships between mold cooling intensities, surface quality of solidified shells, mold heat transfer, and mold flux behavior. As depicted in Figure 11, when the cooling intensity of mold was stronger, the depressions would form due to the uneven infiltration of mold flux melt and greater initial solidification shrinkage of the steel. The thermal stresses in the generated depressions could lead to the formation of thermal cracks. The heat transfer for the initial solidification shell with

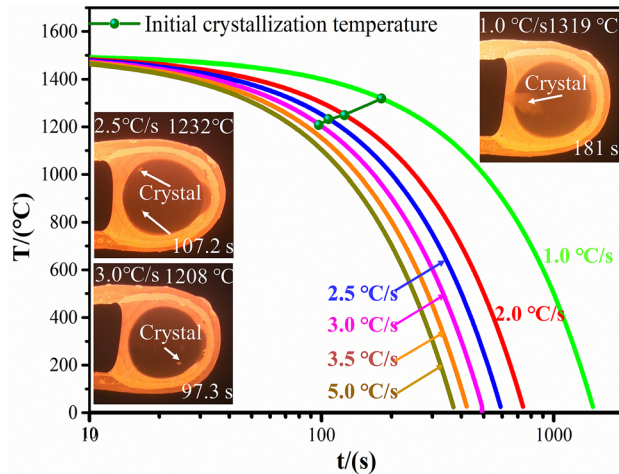


Fig. 10—CCT diagrams and initial crystallization temperature of mold fluxes.

depression decreased significantly during the initial solidification stage under the large mold cooling intensity. In addition, it has been shown that the solidification shrinkage increases with increasing sulfur content.^[14,36] It should be noted that the control of depression-type crack in continuous casting steel using a mold simulator method was not conducted before. The depression and surface crack in the present work are significantly improved in a condition of generally slow mold cooling rate.

IV. CONCLUSIONS

A mold simulator technique was developed to investigate the effects of different mold cooling intensities (3.5, 6.0, 7.5 L/min) on the evolution of depression-type cracks and mold flux infiltration in a steel continuous casting. The main conclusions were drawn as follows:

1. The mold simulator results indicated that when the cooling water flow enhanced from 3.5 to 7.5 L/min, the mean depth of shell surface depressions increased from 90 to 200 μm , and severe longitudinal cracks with lengths ranging from 1722 to 3267 μm formed at the depressions due to the enhancement of thermal stress concentration.
2. Furthermore, as the cooling water flow increased from 3.5 to 7.5 L/min, the average solidification factor of shell increased rapidly from 2.37 to 2.91 $(\text{mm/s})^{1/2}$, and the mean heat flux in the initial solidified shells with depressions reduced by 0.723 MW/m^2 during the 0 to 1.5 seconds stage of the initial solidification.
3. The excessive mold cooling intensities can lead to an uneven infiltration of mold flux melt, the increasing of slag film thickness and appearance of amorphous slag film. The CCT curves results indicated that the

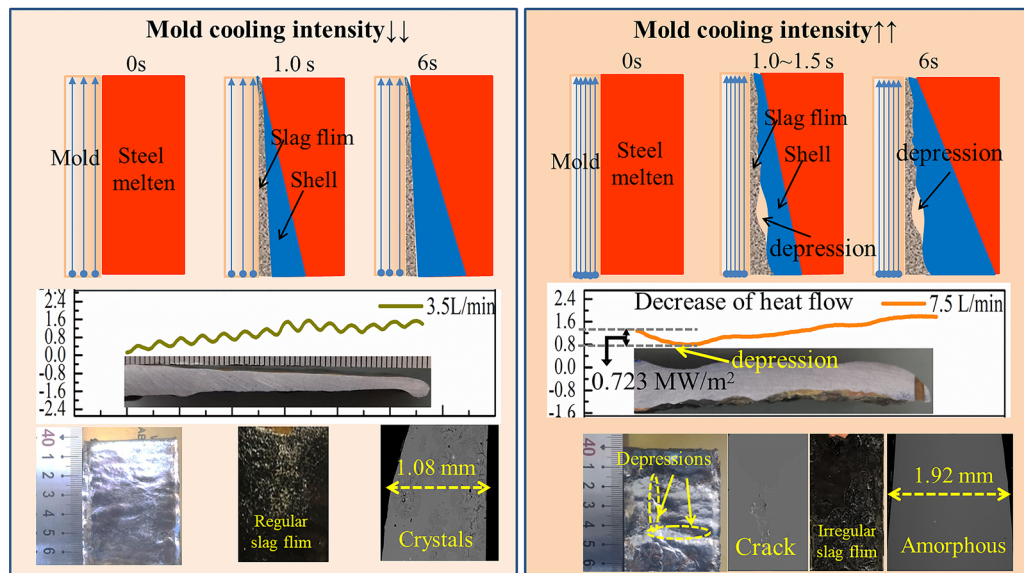


Fig. 11—The formation mechanisms of depression-type cracks for continuous casting steel.

critical cooling rates of glass phase transition for the mold flux was about 3.0 °C/s to 3.5 °C/s.

ACKNOWLEDGMENTS

The financial support for this work from the National Natural Science Foundation of China (Nos. 52274342, 52130408) are gratefully acknowledged.

CONFLICT OF INTEREST

The authors declare that they have no conflict of interest in this paper. All the authors listed have approved the manuscript.

REFERENCES

1. Y. Kim, H. Kim, M. Kang, K. Rhee, S.Y. Shin, and S. Lee: *Metall. Mater. Trans. A*, 2013, vol. 44, pp. 4613–25.
2. Y.T. Guo, Q. Wang, G.J. Chen, and S.P. He: *J. Iron Steel Res. Int.*, 2015, vol. 22(1), pp. 87–92.
3. X.B. Ji, S.X. Zhao, L.M. Fu, J. Peng, J.Q. Gao, D.J. Yu, Z.Z. Huang, and A.D. Shan: *J. Iron Steel Res. Int.*, 2022, vol. 29, pp. 519–28.
4. C. Liang, W.L. Wang, H. He, and J. Zeng: *J. Mater. Res. Technol.*, 2023, vol. 23, pp. 6090–6100.
5. L.D. Xing, Y.P. Bao, M. Wang, and J.H. Yang: *Eng. Fail. Anal.*, 2022, vol. 142, p. 106760.
6. L.D. Xing, X.Y. Fan, M. Wang, L.H. Zhao, and Y.P. Bao: *Metall. Mater. Trans. B*, 2021, vol. 52B, pp. 3208–19.
7. L.D. Xing, M. Wang, J. Guo, Z. Zhang, F. Zeng, B.T. Chen, and Y.P. Bao: *Metals*, 2019, vol. 9, p. 1269.
8. W.L. Wang, S. Luo, Z.Z. Cai, M.Y. Zhu: *Miner. Met. Mater. Soc. (TMS)*, 2013, pp. 89–98.
9. M.M. Wolf: *Iron Steel Soc.*, 1997, vol. 410, p. 15086.
10. J. Cibulka, R. Krzok, R. Hermann, D. Bocek, J. Cupek, and K. Michalek: *Arch. Metall. Mater.*, 2016, vol. 61(1), pp. 283–88.
11. H. Nakato, M. Ozawa, K. Kinoshita, Y. Habu, and T. Emi: *ISIJ Int.*, 1984, vol. 24(11), pp. 957–65.
12. J.K. Brimacombe, F. Weinberg, and E.B. Hawbolt: *Metall. Mater. Trans. B*, 1979, vol. 10B, pp. 279–92.
13. M.L.S. Zappulla: *Mechanisms of Longitudinal Depression Formation in Steel Continuous Casting*, 2020, Colorado School of Mines.
14. J.K. Brimacombe and K. Sorimachi: *Metall. Mater. Trans. B*, 1977, vol. 8B, pp. 489–505.
15. R.B. Mahapatra, J.K. Brimacombe, and I.V. Samarasekera: *Metall. Mater. Trans. B*, 1991, vol. 22B, pp. 875–88.
16. N.F. Zong, L. Yang, and H. Zhang: *Metall. Res. Technol.*, 2017, vol. 114, p. 413.
17. A. Grill and J.K. Brimacombe: *Ironmak. Steelmak.*, 1976, vol. 3, pp. 38–47.
18. H. Murakami, M. Suzuki, T. Kitagawa, and S. Miyahara: *ISIJ Int.*, 1992, vol. 78(1), pp. 105–12.
19. M.L.S. Zappulla and B.G. Thomas: *Mater. Sci. Forum*, 2018, vol. 941, pp. 112–17.
20. M.L.S. Zappulla, L.C. Hibbeler, and B.G. Thomas: *Metall. Mater. Trans. A*, 2017, vol. 48, pp. 3777–93.
21. M.L.S. Zappulla, S.M. Cho, and B.G. Thomas: *Steel Res. Int.*, 2019, vol. 90(4), p. 1800540.
22. M.L.S. Zappulla, S.M. Cho, S. Koric, H.J. Lee, S.H. Kim, and B.G. Thomas: *J. Mater. Process. Technol.*, 2020, vol. 278, p. 116469.
23. M.L.S. Zappulla, B.G. Thomas: *Miner. Met. Mater. Soc. (TMS)*, 2017, pp. 501–10.
24. M. Leng, F. Lai, and J. Li: *Materials*, 2019, vol. 12, pp. 62–74.
25. H. Todoroki, T. Ishii, K. Mizuno, and A. Hongo: *Mater. Sci. Eng. A*, 2005, vol. 413, pp. 121–28.
26. B.G. Thomas, M.S. Jenkins, and R.B. Mahapatra: *Ironmak. Steelmak.*, 2004, vol. 31(6), pp. 485–94.
27. J. Yang, Z.Z. Cai, D.F. Chen, and M.Y. Zhu: *Metall. Mater. Trans. B*, 2019, vol. 50B, pp. 1104–13.
28. H.H. Zhang, W.L. Wang, F.J. Ma, and L.J. Zhou: *Metall. Mater. Trans. B*, 2015, vol. 46B, pp. 2361–73.
29. H.H. Zhang, W.L. Wang, and L.J. Zhou: *Metall. Mater. Trans. B*, 2015, vol. 46B, pp. 2137–52.
30. H.H. Zhang and W.L. Wang: *Metall. Mater. Trans. B*, 2016, vol. 47B, pp. 920–31.
31. H.H. Zhang and W.L. Wang: *Metall. Mater. Trans. B*, 2017, vol. 48B, pp. 779–93.
32. L.D. Xing, Z.F. Zhang, L.H. Zhao, and Y.P. Bao: *Steel Res. Int.*, 2022, vol. 93, p. 2200119.
33. L.D. Xing, Z.F. Zhang, and Y.P. Bao: *J. Mater. Res. Technol.*, 2022, vol. 19, pp. 1367–78.
34. C. Bernhard and G.M. Xia: *Ironmak. Steelmak.*, 2006, vol. 33(1), pp. 52–56.
35. R. Sarkar and Z.S. Li: *Metall. Mater. Trans. B*, 2021, vol. 52B, pp. 1357–78.
36. K.H. Kim, T.J. Yeo, K.H. Oh, and D.N. Lee: *Isij Int.*, 1996, vol. 36, pp. 284–89.

Publisher's Note Springer Nature remains neutral with regard to jurisdictional claims in published maps and institutional affiliations.

Springer Nature or its licensor (e.g. a society or other partner) holds exclusive rights to this article under a publishing agreement with the author(s) or other rightsholder(s); author self-archiving of the accepted manuscript version of this article is solely governed by the terms of such publishing agreement and applicable law.